

Reweighting-annealing method for calculating the value of partition function via quantum Monte Carlo

Yi-Ming Ding,^{1, 2, 3} Jun-Song Sun,⁴ Nvsen Ma,⁴ Gaopei Pan,⁵ Chen Cheng,⁶ and Zheng Yan^{2, 3, *}

¹*State Key Laboratory of Surface Physics and Department of Physics, Fudan University, Shanghai 200438, China*

²*Department of Physics, School of Science and Research Center for*

Industries of the Future, Westlake University, Hangzhou 310030, China

³*Institute of Natural Sciences, Westlake Institute for Advanced Study, Hangzhou 310024, China*

⁴*School of Physics, Beihang University, Beijing 100191, China*

⁵*Institut für Theoretische Physik und Astrophysik and Würzburg-Dresden Cluster of Excellence ct.qmat, Universität Würzburg, 97074 Würzburg, Germany*

⁶*Key Laboratory of Quantum Theory and Applications of MoE, Lanzhou Center for Theoretical Physics, and Key Laboratory of Theoretical Physics of Gansu Province, Lanzhou University, Lanzhou, Gansu 730000, China*

(Dated: May 24, 2024)

Efficient and accurate algorithm for partition function, free energy and thermal entropy calculations is of great significance in statistical physics and quantum many-body physics. Here we present an unbiased but low-technical-barrier algorithm within the quantum Monte Carlo framework, which has exceptionally high accuracy and no systemic error. Compared with the conventional specific heat integral method and Wang-Landau sampling algorithm, our method can obtain a much more accurate result of the sub-leading coefficient of the entropy consistent with CFT. This method can be widely used in both classical and quantum Monte Carlo simulations and is easy to be parallelized on computer.

Introduction.- Quantum Monte Carlo (QMC) is one of the powerful tools in calculating large-scale and high-dimensional quantum many-body systems [1–12]. Although many observables, e.g., energy and specific heat, can be obtained from QMC through sampling the partition function (PF), the value of the PF itself remains difficult to calculate directly. To tackle this problem, the specific heat integral (C-int) method [13] and Wang-Landau (WL) algorithm [14, 15] have been widely adopted to calculate PF and related quantities, such as free energy and entropy. The former method crudely calculates the numerical integration of $S(T) = S(\infty) - \int_T^\infty C(T')/T' dT'$ to obtain the entropy $S(T)$ [16], after which we can calculate PF indirectly. However, this method usually requires a plethora of computational resources to lower the systemic error especially when the specific heat has sharp variation and huge fluctuation. The key idea of the latter method, on the other hand, is to achieve the (effective) density of states of the PF by initially allocating them some default values, then optimizing them to the real ones by flattening some histograms [14, 15, 17]. This method suffers from the problem of error saturation, which prevents us from achieving a result with arbitrary precision, and its convergence is not generally controllable [18, 19].

On the other hand, the high-precision PF and its related quantities, such as free energy and entropy, are significantly important in numerical calculations since it means more effective information. For phase transitions no matter within or beyond the Ginzburg-Landau paradigm, an efficient and accurate way to straightforwardly obtain PF would be crucial, because its (high order) derivative reveals potential phase transitions. The

thermal entropy also relates to the distinctiveness of many novel condensed matters, such as spin ice [20–23], topological order [24–29], fracton phases [30–33], etc. Besides, the precision of entropy can even reveal important intrinsic physics. In conformal field theory (CFT), the prefactor in front of the sub-leading term of entropy often carries universal information [34–44]. Even a small numerical error may make our concerned quantities deviate a lot because the sub-leading term is much more sensitive than the leading one.

In this paper, we present a more accurate and efficient method for calculating PF, dubbed reweight-annealing algorithm, within the framework of Monte Carlo (MC) simulation, either quantum or classical. It is inspired by thermal and quantum annealing algorithm in the quantum simulation area [45–52] and recent developments of the incremental trick in the entanglement calculations of QMC [53–58]. Our method not only has high accuracy for calculating PF, but is unbiased, easy to implement and naturally can be parallelized on computer.

Basic idea.- Given a partition function $Z(\mathbf{p})$, where $\mathbf{p} = [p_1, p_2, \dots]$ denotes the parameters in the PF such as the temperature T and some Hamiltonian parameter s . For example, Fig.1 (a) shows a diagram of the two parameters. For two different parameter points \mathbf{p}' and \mathbf{p}'' , we define the reweighting ratio which can be measured in Monte Carlo

$$\frac{Z(\mathbf{p}')}{Z(\mathbf{p}'')} = \left\langle \frac{W(\mathbf{p}')}{W(\mathbf{p}'')} \right\rangle_{\mathbf{p}''} \quad (1)$$

where $W(\mathbf{p}')$ and $W(\mathbf{p}'')$ denote the weight of the same configuration under different parameters \mathbf{p}' and \mathbf{p}'' , and

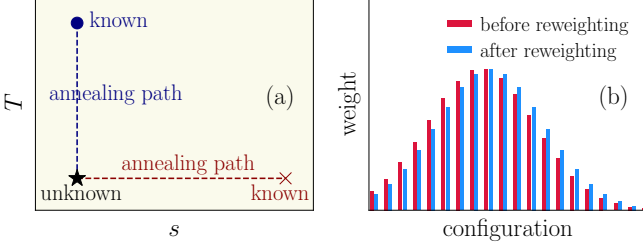


FIG. 1. Schematic diagram of the reweight-annealing method. (a) Finding a reference point and the annealing path connecting the unknown point to it in the parameter space. T and s correspond to the thermal and quantum version, respectively; (b) Using a sampled distribution (red) to represent another distribution (blue) through reweighting a same configuration. If these two distributions are close to each other, the effect of the reweighting would be good since the importance sampling can approximately be kept.

the subscript indicates the result comes from the MC simulation under parameter \mathbf{p}'' . As an example, we take $\mathbf{p} = \beta$, where β denotes the inverse temperature. Under the framework of stochastic series expansion (SSE), we can then derive $Z(\beta')/Z(\beta'') = \langle (\beta'/\beta'')^n \rangle_{\beta''}$, where n is the number of non-identity operators in the SSE simulation. The details of the $Z(\beta')/Z(\beta'')$ have been explained in the supplemental materials (SM).

The second step is to identify a reference point \mathbf{p}_0 , of which the value of $Z(\mathbf{p}_0)$ has already been known. Therefore, by evaluating $Z(\mathbf{p}_0)/Z(\mathbf{p}'')$, we can directly determine the value of $Z(\mathbf{p}'')$. In the example that $\mathbf{p} = \beta$, apparently $Z(0) = d^N$ is pre-knowledge because all the configurations are equally important at infinite high temperature, where N and d are the number of particles and the degree of freedom of a single particle respectively.

However, when \mathbf{p}_0 and \mathbf{p}'' are far away in the parameter space, the value of $Z(\mathbf{p}_0)/Z(\mathbf{p}'')$ would be close to zero or infinity, resulting in the problem of inefficiency and low precision for the MC simulation. This can be easily understood in the reweighting frame as shown in Fig. 1 (b). If we want to use a well-known distribution $Z(\mathbf{p}'') = \sum W(\mathbf{p}'')$ to calculate another distribution $Z(\mathbf{p}') = \sum W(\mathbf{p}')$ via resetting the weight of samplings, the weight before/after the resetting of the same configuration should be close to each other. It is still an importance sampling in this sense and requires that \mathbf{p}' and \mathbf{p}'' should be close enough.

Based on this consideration, practically, we divide the calculation of of Eq. (1) into many steps to enhance precision, i.e.

$$\frac{Z(\mathbf{p}_0)}{Z(\mathbf{p}'')} = \prod_{k=1}^m \frac{Z(\mathbf{p}_{k-1})}{Z(\mathbf{p}_k)} \quad (2)$$

where $\mathbf{p}_m \equiv \mathbf{p}''$ and $Z(\mathbf{p}_{k-1})/Z(\mathbf{p}_k) \rightarrow 1$ as long as $\mathbf{p}_k \rightarrow \mathbf{p}_{k-1}$. Here, \mathbf{p} can be perceived to gradually

change from the point of interest \mathbf{p}'' to the reference point \mathbf{p}_0 along a trajectory (annealing path) in the parameter space, akin to an adiabatic process or annealing as shown in Fig.1 (a). Therefore by calculating Eq. (2), not only we are able to achieve a higher precision of $Z(\mathbf{p}'')$, but concurrently track the variation of PF along this annealing path. This allows us to further analyze the variation of the free energy (and its derivatives) of the system.

Apparently, the annealing path that \mathbf{p} follows determines how large m should we need and how \mathbf{p} varies to perform the calculations of Eq. (2). It can be expected that, similar to conventional thermal annealing or quantum annealing, should the annealing trajectory approach a critical point, an increased number of divisions would be necessary in its vicinity. However, we point out that this actually affects little to our algorithm since numerical simulations only deal with finite system, where the criticality does not result in significant inefficiency. We have also verified this point in our simulations. For example, in the 2D spin-1/2 XXZ model which we present below, where $\mathbf{p} = T$ is the temperature, we implemented an equal division strategy with step size $\Delta T = 0.01$. With 20000 Monte Carlo samples for each bin, we are able to achieve a sufficiently smooth curve for further numerical differentiation. More discussions about the segmentation are in the section of “Dynamical annealing process”.

Thermal and quantum reweight-annealing- As it shown in Fig. 1, if $\mathbf{p} = \beta$, as previously mentioned, the annealing path connects an unknown inverse temperature point β'' to the infinite temperature point β_0 , which serves as the reference. For convenience, we call this kind of process the thermal reweight-annealing (T-Re-An). Similarly, we can consider the so-called quantum reweight-annealing (Q-Re-An) by setting $\mathbf{p} = s$, where s comes from $H(s) = sH_0 + (1-s)H_1$, which is the archetypal Hamiltonian of quantum annealing with $Z(s) = e^{-\beta H(s)}$. Here, H_1 correspond to our reference point $s = 0$, and we would like to obtain the PF related to H_0 . We emphasize that different from the thermal version, the choice of H_1 here is much more flexible. For example, we can take $H_1 = \sum_i \sigma_i^x$. Then at the zero temperature ($\beta \rightarrow \infty$), H_1 only has a unique ground state, thus its thermal entropy is minimized to be zero, resulting in $\ln Z(0) = -\lim_{\beta \rightarrow \infty} \beta E$, where $E = -N$ is the ground state energy of H_1 . More details about the T-Re-An and Q-Re-An scheme can be found in the SM.

Dynamical annealing process.- For the thermal and quantum reweight-annealing schemes, we provide a dynamical strategy to automatically regulate the alteration of \mathbf{p} throughout the annealing process. This not only serves as an economic way for the division in Eq. (2), but can avoid the problem of precision loss when different $r(\mathbf{p}_{k-1}, \mathbf{p}_k)$ differ by several orders of magnitude in the computer. For demonstration, we only discuss the thermal case, i.e. $\mathbf{p} = \beta$, in this section.

Without loss of generality, we assume $\beta_{k-1} < \beta_k$ in

Eq. (2), and define the rate $\alpha_k \equiv \beta_{k-1}/\beta_k < 1$. Within the framework of SSE, we have

$$\frac{Z(\beta_{k-1})}{Z(\beta_k)} = \langle \alpha_k^{n_k} \rangle_{\beta_k} \quad (3)$$

where n_k is the number of all non-identity operators in the SSE simulation, and the subscript β_k denotes that this simulation is performed at the parameter point β_k .

The annealing process starts from $k = m$, and we require $Z(\beta_{k-1})/Z(\beta_k) = \epsilon < 1$, where the choice of ϵ should match N_{MC} , the number of MC steps we use for samplings, as the error in MC simulations is proportional to $1/\sqrt{N_{MC}}$. Next, we set $n_k \approx \tilde{n}_k = \Lambda_k \beta_k L$ ($\Lambda_k \beta_k L^2$) for 1D (2D) system, and Λ_k can be ascertained through the examination of result convergence. This comes from the fact that in SSE, the energy satisfies $E_k = -\langle n_k \rangle / \beta_k$. Practically, we set Λ_k to be the same for all k for convenience. This strategy not only makes $Z(\beta_{k-1})/Z(\beta_k) \approx \epsilon$ for all k , but determines the next step in the annealing path, i.e. $\beta_{k-1} = \alpha_k \beta_k$. The division will be more sparse when β gets smaller as we expected, where the thermal fluctuation has destroyed any order and $Z(\beta_{k-1})/Z(\beta_k) \rightarrow 1$, which has little contribution to the result. Apparently, this strategy naturally allows for parallelization of evaluating different $Z(\beta_{k-1})/Z(\beta_k)$ in Eq. (2). It is also easy to calculate that the number of divisions is around $(\beta - \beta_0) \Lambda L / |\ln \epsilon|$ for large L or $(\beta - \beta_0)$, where $\Lambda_k = \Lambda$ for all k . Therefore, this dynamical annealing strategy does not require exponentially increasing number of divisions.

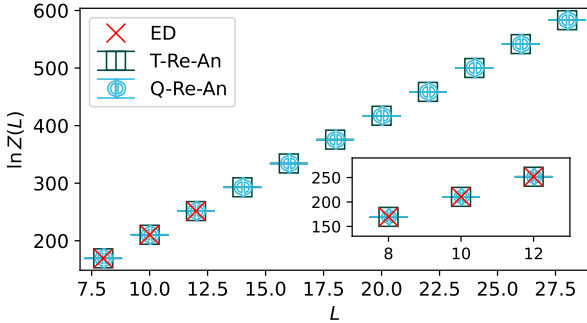


FIG. 2. For $\beta = 30$, the values of $\ln Z$ as a function of the chain length L , where both T-Re-An method and Q-Re-An method have a perfect match with ED. For example, for $L = 12$, the results from the two methods are 251.625(2) and 251.624(2), respectively, and the exact result is 251.62283 from ED calculations. Attention that here in practical SSE simulations, the Hamiltonian has a energy shift of $-1/4$ for each two-body term.

1D spin-1/2 Heisenberg chain. As the first example, we consider an 1D spin-1/2 antiferromagnetic (AFM) Heisenberg chain with periodic boundary condition (PBC) with $\beta = 30$ and length L . We use both the T-Re-An method and the Q-Re-An method to calculate

the PF. For the quantum version, we write

$$H(s) = s \left[\sum_i \mathbf{S}_i \cdot \mathbf{S}_{i+1} \right] + (1-s) \left[\sum_{i \in \text{even}} \mathbf{S}_i \cdot \mathbf{S}_{i+1} \right] \quad (4)$$

where $H_0 = \sum_i \mathbf{S}_i \cdot \mathbf{S}_{i+1}$ and $H_1 = \sum_{i \in \text{even}} \mathbf{S}_i \cdot \mathbf{S}_{i+1}$. Apparently, the unique ground state of H_1 is a tensor product of $L/2$ singlets, each carrying energy $-3/4$ ($\hbar = 1$). The estimator for $Z(s')/Z(s'')$ is $\langle (s'/s'')^{n_{\text{odd}}} \rangle_{s''}$ in this model, with n_{odd} denoting the amount of non-identity operators acting on all the bonds with odd indices within the framework of SSE. As it is shown in Fig. 2, both the results of T-Re-An and Q-Re-An method can match that of the exact diagonalization (ED) method exceptionally well for small lengths, which verify the validity of our methods. The results are also consistent with the expectation that $\ln Z \propto L + o(L)$, where $o(L)$ means higher order terms which is negligible compared with L . One may feel this example too trivial and easy to be calculated. Therefore we introduce the second example which needs a high-precision to extract the correction of the sub-leading term in entropy.

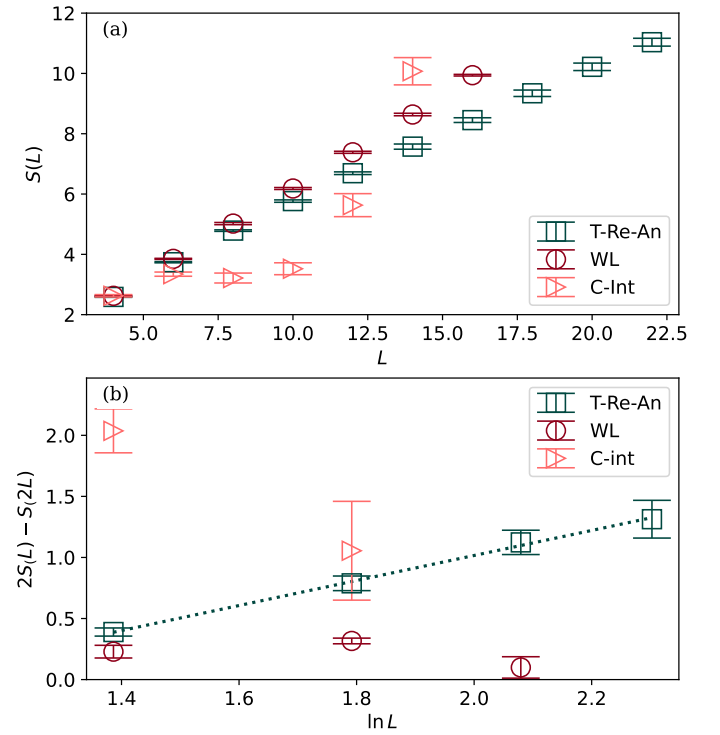


FIG. 3. (a) Thermodynamic entropies $S(L)$ as a function of L calculated from different algorithms; (b) The $\ln L$ term extracted by calculating $2S(L) - S(2L)$, and the fitting slope (dashed green line) here is $1.00(2)$.

2D LBW-HM. To further exploit the advantage of our method, we calculate the thermodynamic entropy of a 2D lattice Bisognano-Wichmann Heisenberg model (LBW-HM) [59, 60], the thermodynamic entropy S of which at $\beta = 1$ provides a good approximation for the Von

Neumann entanglement entropy of a 2D PBC square lattice spin-1/2 AFM Heisenberg model under smooth bipartition [61, 62]. According to the CFT prediction and previous numerical results [55, 63–65], the coefficient of sub-leading term of the entropy reflects the number of Goldstone modes. Here, the thermal entropy of the LBW-HM at $\beta = 1$ should obey $S(L) = aL + b\ln L + c$, and $b = n_G/2$, where $n_G = 2$ is the number of Goldstone modes of the 2D spin-1/2 AFM Heisenberg model [64, 66]. In this context, coarse result of entropy is disfavored because the the coefficient b in front of the sub-leading term is sensitive to errors. We have compared our method with the specific heat integral (C -int) and Wang-Landau (WL) algorithm in this example.

Similar to our method, the C -int method also depends on how many intervals we divide for β . Therefore we take the same division and Monte Carlo steps to compare the performance of these two algorithms. As it shown in Fig. 3, the C -int method has great systemic error because the number of division is adequate for our method, but not the C -int method, indicating more computational resources needed for it to achieve better accuracy.

For the WL algorithm, on another hand, the allocation of total computational resources should not be predetermined as it hinges on when we can achieve a converged and flat histogram. Fig. 3 shows great error of the results obtained from the vanilla WL samplings [15]. This reflects the problem of error saturation, which is intrinsic in this algorithm due to an approximately flat histogram and the empirical refinement parameter [18, 19, 67]. Another disadvantage of the WL sampling compared with our method is that it cannot be parallelized: the two subroutines for flattening the corresponding histograms before and after an adjustment of the refinement parameter, must be executed sequentially. To achieve an arbitrary precision within the Wang-Landau framework is not easy. In contrast, our method is much more accessible as we only need to measure the observable of $Z(\mathbf{p}_{k-1})/Z(\mathbf{p}_k)$ in many conventional and mature MC algorithms.

2D XXZ model.– As the last example, we consider a much more complex model, a 2D spin-1/2 XXZ model with next nearest neighbor interaction,

$$H = - \sum_{\langle i,j \rangle} [2S_i^z S_j^z + S_i^x S_j^x + S_i^y S_j^y] - 0.2 \sum_{\langle\langle i,j \rangle\rangle} [2S_i^z S_j^z + S_i^x S_j^x + S_i^y S_j^y]. \quad (5)$$

where $\langle i,j \rangle$ and $\langle\langle i,j \rangle\rangle$ denotes the nearest and the next nearest neighbors respectively. The lattice we simulated is a square lattice with PBC. This model has a finite temperature 2D Ising phase transition which can be captured by the second or higher order derivative of the free energy $F = -T \ln Z$.

For convenience, here we use equal distance of $T = 1/\beta = 0.01$ to implement our Re-An method, and it is

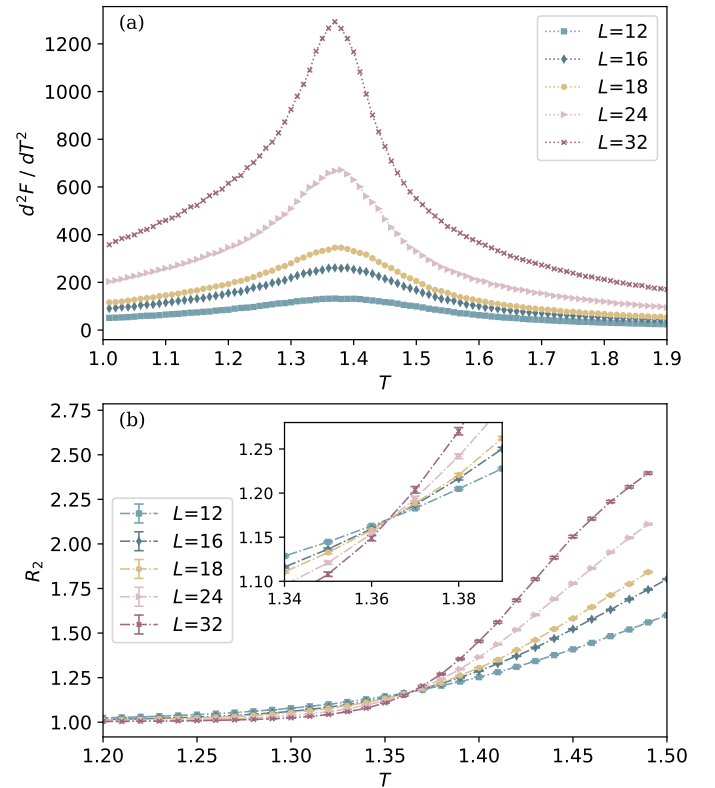


FIG. 4. (a) The second order derivative of the free energy, d^2F/dT^2 , changes with the temperature T in different system size. The peak diverges more when the size becomes larger, which probes the phase transition point here; (b) The Binder ratios in this model at different sizes intersecting at a point which is highly consistent with the peak obtained by Re-An algorithm.

also easy for numerical differentiation. Because a constant factor of the PF does not affect the (higher order) derivative of F , thus we choose $Z(T^* = 1.95)$ as the reference to replace annealing to a known point. The PF we gained is actually $Z(T)/Z(T^*)$ where $Z(T^*)$ is an unknown constant. Then we indeed observe a divergent peak of the second order derivative of the free energy as shown in Fig. 4(a), which accurately probes the phase transition point, matching with the intersection point of Binder ratios $R_2 = \langle M^4 \rangle / \langle M^2 \rangle^2$ of different sizes shown in Fig. 4(b), where M denotes the magnetization.

This example also inspires us that **connecting to a known point is not necessary when we just need the second or higher order derivative of free energy**. The data also demonstrate the high-precision of our method, where the second order derivative is still smooth and precise.

Summary.– We propose an unbiased algorithm within Monte Carlo framework, which has low-technical barrier and no systemic error. The method can be easily implemented for parallel computation and can obtain the value of partition function, free energy and thermal entropy

with high precision. **The method has two keynotes:** (1) Find a parameter path in whole space (either temperature or external parameter) connecting a known point and the to-be-solved one. If we only want to calculate the (high order) derivative of the PF, even fixing an unknown point as the reference is enough; (2) Annealing along the path to calculate the final result through a propagation formula.

We show the advantage of our method via calculating the thermal entropy of 2D LBW-HM and successfully extract precise coefficient of the sub-leading term ($\ln L$), which is consistent with the CFT prediction and catch the correct number of Goldstone modes. In comparison, the *C*-int and the WL sampling both have worse performance. In a 2D XXZ model, the numerical second derivative of the Re-An data is still smooth and precise, which accurately probes the phase transition point. Our method make the efficient and high-precision calculation of entropy and other related physical quantities accessible, which can reveal some universal information, such as CFT, criticality and symmetry breaking.

Acknowledgement.— We acknowledge the start-up funding of Westlake University. The authors also acknowledge Beijing PARATERA Tech Co.,Ltd. (<https://www.paratera.com/>) for providing HPC resources that have contributed to the research results reported within this paper. CC and ZY thank the support of the National Natural Science Foundation of China (grant nos. 12174167, 12247101).

* zhengyan@westlake.edu.cn

[1] Anders W. Sandvik, “Stochastic series expansion method with operator-loop update,” *Phys. Rev. B* **59**, R14157–R14160 (1999).

[2] Anders W. Sandvik, “Computational Studies of Quantum Spin Systems,” *AIP Conference Proceedings* **1297**, 135–338 (2010).

[3] Anders W. Sandvik, “Stochastic series expansion methods,” (2019), arXiv:1909.10591 [cond-mat.str-el].

[4] O. F. Syljuåsen and A. W. Sandvik, *Phys. Rev. E* **66**, 046701 (2002).

[5] Zheng Yan, Yongzheng Wu, Chenrong Liu, Olav F. Syljuåsen, Jie Lou, and Yan Chen, “Sweeping cluster algorithm for quantum spin systems with strong geometric restrictions,” *Phys. Rev. B* **99**, 165135 (2019).

[6] Masuo Suzuki, Seiji Miyashita, and Akira Kuroda, “Monte carlo simulation of quantum spin systems. i,” *Progress of Theoretical Physics* **58**, 1377–1387 (1977).

[7] J. E. Hirsch, R. L. Sugar, D. J. Scalapino, and R. Blankenbecler, “Monte carlo simulations of one-dimensional fermion systems,” *Phys. Rev. B* **26**, 5033–5055 (1982).

[8] Masuo Suzuki, “Relationship between d-dimensional quantal spin systems and (d+ 1)-dimensional ising systems: Equivalence, critical exponents and systematic approximants of the partition function and spin correlations,” *Progress of theoretical physics* **56**, 1454–1469 (1976).

[9] Henk W. J. Blöte and Youjin Deng, “Cluster monte carlo simulation of the transverse ising model,” *Phys. Rev. E* **66**, 066110 (2002).

[10] Chun-Jiong Huang, Longxiang Liu, Yi Jiang, and Youjin Deng, “Worm-algorithm-type simulation of the quantum transverse-field ising model,” *Phys. Rev. B* **102**, 094101 (2020).

[11] Zhijie Fan, Chao Zhang, and Youjin Deng, “Clock factorized quantum monte carlo method for long-range interacting systems,” (2023), arXiv:2305.14082 [physics.comp-ph].

[12] Zheng Yan, “Global scheme of sweeping cluster algorithm to sample among topological sectors,” *Phys. Rev. B* **105**, 184432 (2022).

[13] Patrick Emonts and Stefan Wessel, “Monte carlo study of the discontinuous quantum phase transition in the transverse-field ising model on the pyrochlore lattice,” *Phys. Rev. B* **98**, 174433 (2018).

[14] Fugao Wang and D. P. Landau, “Efficient, multiple-range random walk algorithm to calculate the density of states,” *Phys. Rev. Lett.* **86**, 2050–2053 (2001).

[15] Matthias Troyer, Stefan Wessel, and Fabien Alet, “Flat histogram methods for quantum systems: Algorithms to overcome tunneling problems and calculate the free energy,” *Phys. Rev. Lett.* **90**, 120201 (2003).

[16] *T* means the temperature and *C* is the specific heat. Entropy at infinite temperature $S(\infty)$ is known because each configuration has equal weight.

[17] P. M. C. de Oliveira, T. J. P. Penna, and H. J. Herrmann, “Broad histogram method,” (1996), arXiv:cond-mat/9610041.

[18] R. E. Belardinelli and V. D. Pereyra, “Wang-Landau algorithm: A theoretical analysis of the saturation of the error,” *The Journal of Chemical Physics* **127**, 184105 (2007), https://pubs.aip.org/aip/jcp/article-pdf/doi/10.1063/1.2803061/14890498/184105_1_online.pdf.

[19] Chenggang Zhou and R. N. Bhatt, “Understanding and improving the wang-landau algorithm,” *Phys. Rev. E* **72**, 025701 (2005).

[20] J Snyder, JS Slusky, RJ Cava, and P Schiffer, “How ‘spin ice’freezes,” *Nature* **413**, 48–51 (2001).

[21] Sandra H Skjærvø, Christopher H Marrows, Robert L Stamps, and Laura J Heyderman, “Advances in artificial spin ice,” *Nature Reviews Physics* **2**, 13–28 (2020).

[22] Masafumi Udagawa, Ludovic Jaubert, *et al.*, *Spin Ice* (Springer, 2021).

[23] Steven T Bramwell and Mark J Harris, “The history of spin ice,” *Journal of Physics: Condensed Matter* **32**, 374010 (2020).

[24] Hong-Chen Jiang, Zhenghan Wang, and Leon Balents, “Identifying topological order by entanglement entropy,” *Nature Physics* **8**, 902–905 (2012).

[25] C Castelnovo, R Moessner, and Shivaji Lal Sondhi, “Spin ice, fractionalization, and topological order,” *Annu. Rev. Condens. Matter Phys.* **3**, 35–55 (2012).

[26] Subir Sachdev, “Topological order, emergent gauge fields, and fermi surface reconstruction,” *Reports on Progress in Physics* **82**, 014001 (2018).

[27] Michael Levin and Xiao-Gang Wen, “Detecting topological order in a ground state wave function,” *Phys. Rev. Lett.* **96**, 110405 (2006).

[28] Zheng Yan, Yan-Cheng Wang, Nvsen Ma, Yang Qi, and

Zi Yang Meng, "Topological phase transition and single/multi anyon dynamics of z 2 spin liquid," *npj Quantum Materials* **6**, 39 (2021).

[29] Zheng Yan, Rhine Samajdar, Yan-Cheng Wang, Subir Sachdev, and Zi Yang Meng, "Triangular lattice quantum dimer model with variable dimer density," *Nature Communications* **13**, 5799 (2022).

[30] Michael Pretko, Xie Chen, and Yizhi You, "Fracton phases of matter," *International Journal of Modern Physics A* **35**, 2030003 (2020).

[31] Rahul M Nandkishore and Michael Hermele, "Fractons," *Annual Review of Condensed Matter Physics* **10**, 295–313 (2019).

[32] Andrey Gromov and Leo Radzihovsky, "Colloquium: Fracton matter," *Rev. Mod. Phys.* **96**, 011001 (2024).

[33] Chengkang Zhou, Meng-Yuan Li, Zheng Yan, Peng Ye, and Zi Yang Meng, "Evolution of dynamical signature in the x-cube fracton topological order," *Phys. Rev. Res.* **4**, 033111 (2022).

[34] Pasquale Calabrese and Alexandre Lefevre, "Entanglement spectrum in one-dimensional systems," *Phys. Rev. A* **78**, 032329 (2008).

[35] Eduardo Fradkin and Joel E. Moore, "Entanglement entropy of 2d conformal quantum critical points: Hearing the shape of a quantum drum," *Phys. Rev. Lett.* **97**, 050404 (2006).

[36] Zohar Nussinov and Gerardo Ortiz, "Sufficient symmetry conditions for Topological Quantum Order," *Proc. Nat. Acad. Sci.* **106**, 16944–16949 (2009).

[37] Zohar Nussinov and Gerardo Ortiz, "A symmetry principle for topological quantum order," *Annals Phys.* **324**, 977–1057 (2009).

[38] H. Casini and M. Huerta, "Universal terms for the entanglement entropy in 2+1 dimensions," *Nuclear Physics B* **764**, 183–201 (2007).

[39] Wenjie Ji and Xiao-Gang Wen, "Noninvertible anomalies and mapping-class-group transformation of anomalous partition functions," *Phys. Rev. Research* **1**, 033054 (2019).

[40] Wenjie Ji and Xiao-Gang Wen, "Categorical symmetry and noninvertible anomaly in symmetry-breaking and topological phase transitions," *Phys. Rev. Research* **2**, 033417 (2020).

[41] Liang Kong, Tian Lan, Xiao-Gang Wen, Zhi-Hao Zhang, and Hao Zheng, "Algebraic higher symmetry and categorical symmetry: A holographic and entanglement view of symmetry," *Phys. Rev. Research* **2**, 043086 (2020).

[42] Xiao-Chuan Wu, Wenjie Ji, and Cenke Xu, "Categorical symmetries at criticality," *Journal of Statistical Mechanics: Theory and Experiment* **2021**, 073101 (2021).

[43] Jiarui Zhao, Zheng Yan, Meng Cheng, and Zi Yang Meng, "Higher-form symmetry breaking at ising transitions," *Phys. Rev. Research* **3**, 033024 (2021).

[44] Xiao-Chuan Wu, Chao-Ming Jian, and Cenke Xu, "Universal Features of Higher-Form Symmetries at Phase Transitions," *SciPost Phys.* **11**, 33 (2021).

[45] David A. Huse and Daniel S. Fisher, "Residual energies after slow cooling of disordered systems," *Phys. Rev. Lett.* **57**, 2203–2206 (1986).

[46] Giuseppe E. Santoro, Roman Martoňák, Erio Tosatti, and Roberto Car, "Theory of quantum annealing of an Ising spin glass," *Science* **295**, 2427–2430 (2002).

[47] Andrew Lucas, "Ising formulations of many NP problems," *Front. Phys.* **2**, 5 (2014).

[48] Tadashi Kadowaki and Hidetoshi Nishimori, "Quantum annealing in the transverse ising model," *Phys. Rev. E* **58**, 5355–5363 (1998).

[49] Marc Mézard and Andrea Montanari, *Information, Physics, and Computation* (Oxford University Press, 2009).

[50] Bettina Heim, Troels F. Rønnow, Sergei V. Isakov, and Matthias Troyer, "Quantum versus classical annealing of Ising spin glasses," *Science* **348**, 215–217 (2015).

[51] Zheng Yan, Zheng Zhou, Yan-Hua Zhou, Yan-Cheng Wang, Xingze Qiu, Zi Yang Meng, and Xue-Feng Zhang, "Quantum optimization within lattice gauge theory model on a quantum simulator," *npj Quantum Information* **9**, 89 (2023).

[52] Yi-Ming Ding, Yan-Cheng Wang, Shi-Xin Zhang, and Zheng Yan, "Quantum imaginary time evolution and quantum annealing meet topological sector optimization," *arXiv preprint arXiv:2310.04291* (2023).

[53] Vincenzo Alba, "Out-of-equilibrium protocol for rényi entropies via the jarzynski equality," *Phys. Rev. E* **95**, 062132 (2017).

[54] Jonathan D'Emidio, "Entanglement entropy from nonequilibrium work," *Phys. Rev. Lett.* **124**, 110602 (2020).

[55] Jiarui Zhao, Bin-Bin Chen, Yan-Cheng Wang, Zheng Yan, Meng Cheng, and Zi Yang Meng, "Measuring rényi entanglement entropy with high efficiency and precision in quantum monte carlo simulations," *npj Quantum Materials* **7**, 69 (2022).

[56] Jiarui Zhao, Yan-Cheng Wang, Zheng Yan, Meng Cheng, and Zi Yang Meng, "Scaling of entanglement entropy at deconfined quantum criticality," *Phys. Rev. Lett.* **128**, 010601 (2022).

[57] Gaopei Pan, Yuan Da Liao, Weilun Jiang, Jonathan D'Emidio, Yang Qi, and Zi Yang Meng, "Stable computation of entanglement entropy for two-dimensional interacting fermion systems," *Phys. Rev. B* **108**, L081123 (2023).

[58] Xuan Zhou, Zi Yang Meng, Yang Qi, and Yuan Da Liao, "Incremental swap operator for entanglement entropy: Application for exponential observables in quantum monte carlo simulation," *arXiv preprint arXiv:2401.07244* (2024).

[59] G. Giudici, T. Mendes-Santos, P. Calabrese, and M. Dalmonte, "Entanglement hamiltonians of lattice models via the bisognano-wichmann theorem," *Phys. Rev. B* **98**, 134403 (2018).

[60] M. Dalmonte, B. Vermersch, and P. Zoller, "Quantum simulation and spectroscopy of entanglement hamiltonians," *Nature Physics* **14**, 827–831 (2018).

[61] T. Mendes-Santos, G. Giudici, M. Dalmonte, and M. A. Rajabpour, "Entanglement hamiltonian of quantum critical chains and conformal field theories," *Phys. Rev. B* **100**, 155122 (2019).

[62] T Mendes-Santos, G Giudici, R Fazio, and M Dalmonte, "Measuring von neumann entanglement entropies without wave functions," *New Journal of Physics* **22**, 013044 (2020).

[63] Max A. Metlitski and Tarun Grover, "Entanglement entropy of systems with spontaneously broken continuous symmetry," (2015), *arXiv:1112.5166 [cond-mat.str-el]*.

[64] Nicolas Laflorencie, "Quantum entanglement in condensed matter systems," *Physics Reports* **646**, 1–59 (2016).

- [65] Zehui Deng, Lu Liu, Wenan Guo, and H. Q. Lin, “Improved scaling of the entanglement entropy of quantum antiferromagnetic heisenberg systems,” Phys. Rev. B **108**, 125144 (2023).
- [66] Max A. Metlitski and Tarun Grover, “Entanglement entropy of systems with spontaneously broken continuous symmetry,” (2011), arXiv:1112.5166.
- [67] R. E. Belardinelli, S. Manzi, and V. D. Pereyra, “Analysis of the convergence of the 1t and wang-landau algorithms in the calculation of multidimensional integrals,” Phys. Rev. E **78**, 067701 (2008).

SUPPLEMENTAL MATERIAL

(I) Estimators in thermal and quantum reweight-annealing under the SSE framework

For the thermal case, the estimator of $Z(\beta')/Z(\beta'')$ is general, which is

$$\begin{aligned} \frac{Z(\beta')}{Z(\beta'')} &= \frac{1}{Z(\beta'')} \text{tr}\{e^{-\beta' H}\} \\ &= \frac{1}{Z(\beta'')} \text{tr}\left\{\sum_n \left(\frac{\beta'}{\beta''}\right)^n \frac{(\beta'')^n}{n!} (-H)^n\right\} \quad (1) \\ &= \left\langle \left(\frac{\beta'}{\beta''}\right)^n \right\rangle_{\beta''} \end{aligned}$$

and the subscript denotes that this simulation should be performed at the inverse temperature β'' .

For the quantum case with $H(s) = sH_0 + (1-s)H_1 = H_1 + s(H_0 - H_1)$, $Z(s')/Z(s'')$ usually takes the form $\langle (s'/s'')^{n_s} \rangle_{s''}$ within the framework of SSE, where n_s is the number of non-identity operators related to $(H_0 - H_1)$. For instance, if

$$\begin{aligned} H(s) &= s \left[\sum_i \mathbf{S}_i \cdot \mathbf{S}_{i+1} \right] + (1-s) \left[\sum_{i \in \text{even}} \mathbf{S}_i \cdot \mathbf{S}_{i+1} \right] \quad (2) \\ &= \sum_{i \in \text{even}} \mathbf{S}_i \cdot \mathbf{S}_{i+1} + s \left[\sum_{i \in \text{odd}} \mathbf{S}_i \cdot \mathbf{S}_{i+1} \right] \end{aligned}$$

where $H_0 = \sum_i \mathbf{S}_i \cdot \mathbf{S}_{i+1}$ and $H_1 = \sum_{i \in \text{even}} \mathbf{S}_i \cdot \mathbf{S}_{i+1}$, then

$$\begin{aligned} \frac{Z(s')}{Z(s'')} &= \frac{1}{Z(s'')} \text{tr}\{e^{-\beta H(s')}\} \\ &= \frac{1}{Z(s'')} \sum_{\alpha, S_M} \left(\frac{s'}{2}\right)^{n_{\text{odd}}} \left(\frac{1}{2}\right)^{n_{\text{even}}} \tilde{S}_{\alpha, M} \\ &= \frac{1}{Z(s'')} \sum_{\alpha, S_M} \left(\frac{s'}{s''}\right)^{n_{\text{odd}}} \left(\frac{s''}{2}\right)^{n_{\text{odd}}} \left(\frac{1}{2}\right)^{n_{\text{even}}} \tilde{S}_{\alpha, M} \\ &= \left\langle \left(\frac{s'}{s''}\right)^{n_{\text{odd}}} \right\rangle_{s''} \quad (3) \end{aligned}$$

where n_{odd} (n_{even}) denotes the amounts of non-identity operators acting on the bonds with odd (even) indices in SSE simulation, and

$$\tilde{S}_{\alpha, M} = \frac{\beta^n (M-n)!}{M!} \prod_{i=1}^M \langle \alpha_{i-1} | H_{a_i, b_i} | \alpha_i \rangle \quad (4)$$

corresponds to operator string S_M and the propagated states $\{\alpha_0, \alpha_1, \dots, \alpha_M\}$ along the axis of imaginary time.

(II) Technical details of the annealing process

For the thermal and quantum reweight-annealing scheme with a scalar parameter p , our target is to com-

pute

$$\frac{Z(p_0)}{Z(p)} = \left\langle \frac{W(p_0)}{W(p)} \right\rangle_p \quad (5)$$

where p_0 is the reference point in the parameter space. For the models we consider, $p_0 = 0$. Practically, we take p_0 to be a sufficiently small number (e.g. 10^{-8} in our paper) in the computer. The adequacy can be checked by comparing the results with that of a smaller p_0 so as to see whether the results converge.

We first take $p = \beta$ for illustration and the case that $p = s$ is similar. The difference will be clarified at the end of this section. Without loss of generality, we assume $\beta_0 < \beta$. In case that β_0 and β are far away in the parameter space, to ensure importance sampling, we divide $[\beta_0, \beta]$ into m intervals $[\beta_0, \beta_1], [\beta_1, \beta_2], \dots, [\beta_{m-1}, \beta_m]$, where $\beta_m \equiv \beta$, i.e.

$$\frac{Z(\beta_0)}{Z(\beta)} = \prod_{k=1}^m \frac{Z(\beta_{k-1})}{Z(\beta_k)} \quad (6)$$

Each interval $[\beta_{k-1}, \beta_k]$ ought to be sufficiently narrow so that the distribution at β_k can well samples the configurations at β_{k-1} . Otherwise, the sampling process would be inefficient. Then the natural questions following are how to partition $[\beta_0, \beta]$ and the how many intervals we need for Eq. (6)

It can be expected that if β_k and β_{k-1} are separated on the two sides of the critical point, we may need a bulk of samples to estimate $Z(\beta_{k-1})/Z(\beta_k)$. However, we point out that this actually affects little to our algorithm since numerical simulations only deal with finite system, where the criticality does not result in significant inefficiency. We have also verified this point in our simulations. For example, in the 2D spin-1/2 XXZ model, we implemented an equal division strategy with step size $\Delta T = 0.01$. With 20000 Monte Carlo samples for each bin, we were able to achieve a sufficiently smooth curve for further numerical differentiation. However, the strategy that we divide $[\beta_0, \beta]$ into equal intervals or a geometric progression is not economic. We can expect that when $\beta \rightarrow 0$ (approaching infinite high temperature), the division can be more sparse compared to that at low temperatures. Therefore, an economic strategy to divide the interval is needed.

In addition to the division problem, $Z(\beta_0)/Z(\beta)$ could be an exponentially small number exceeding the data range of computer (e.g. $1.7 \times 10^{-308} \sim 1.7 \times 10^{308}$ for double type data), and we should store $\ln[Z(\beta_0)/Z(\beta)]$ in the computer. However, simply applying the logarithm to Eq. (6) and converting the multiplication to addition may lead to precision loss in computer calculations if $\ln[Z(\beta_{k-1})/Z(\beta_k)]$ and $\ln[Z(\beta_k)/Z(\beta_{k+1})]$ differ by several orders of magnitude.

To address the two problems above, we present a dynamical approach here. Define $\alpha_k \equiv \beta_{k-1}/\beta_k < 1$, and

within the framework of SSE, we have

$$\frac{Z(\beta_{k-1})}{Z(\beta_k)} = \langle \alpha_k^{n_k} \rangle_{\beta_k} \quad (7)$$

where n_k is the number of all non-identity operators in the SSE simulation. Our dynamical process then starts from the last point with $k = m$, and we require

$$\frac{Z(\beta_{k-1})}{Z(\beta_k)} = \epsilon < 1, \quad (8)$$

where the choice of ϵ should match N_{MC} , the number of MC steps we use for samplings, as the error in MC simulations is proportional to $1/\sqrt{N_{MC}}$.

Next, we set $n_k \approx \tilde{n}_k = \Lambda_k \beta_k L$ ($\Lambda_k \beta_k L^2$) for 1D (2D) system, and Λ_k can be ascertained through the examination of result convergence. This comes from the fact that in SSE, the energy satisfies $E_k = -\langle n_k \rangle / \beta_k$. Practically, we set Λ_k to be the same for all k for convenience. Then $Z(\beta_{k-1})/Z(\beta_k)$ can be obtained from the simulation from

$$\langle \alpha_k^{n_k} \rangle = \langle (\epsilon^{1/\tilde{n}_k})^{n_k} \rangle_{\beta_k} \approx \epsilon, \quad \beta_{k-1} = \alpha_k \beta_k \quad (9)$$

Eq. (9) not only requires $Z(\beta_{k-1})/Z(\beta_k) \approx \epsilon$ for all k , but determines the next step in the annealing path. Therefore, with this dynamical annealing strategy, the division will be more sparse when β gets smaller.

This strategy actually requires the number divisions of scale proportional to the system size for large systems. For the 1D system as an example,

$$\beta_{k-1} = \epsilon^{\frac{1}{\Lambda \beta_k L}} \beta_k \approx \left(1 + \frac{\ln \epsilon}{\Lambda \beta_k L} \right) \beta_k \quad (10)$$

or

$$\beta_k - \beta_{k-1} = -\frac{\ln \epsilon}{\Lambda L} \quad (11)$$

then the number of divisions is around $(\beta - \beta_0) \Lambda L / |\ln \epsilon|$.

One more thing we have to pay attention is that when $\beta \rightarrow 0$, we have $\alpha_k \rightarrow 0$, which will also exceed the range of a number saved in the computer. Therefore we manually set a lower bound for α_k (e.g. $\min \alpha_k = \epsilon$ in our simulation). The existence of lower bound makes the division in the region that $\beta \rightarrow 0$ denser than that Eq. (9) requires. Since most $Z(\beta_{k-1})/Z(\beta_k)$ still at the same order of magnitude, e.g. $\epsilon = 10^{-2}$ used for the first two example in our simulation, and the more divisions when $\beta \rightarrow 0$ only constitutes a very small proportion, this affects little to the precision. In Fig. 1, we plot the number of divisions in the T-Re-An method of first example in our paper for reference, where we take $\Lambda = L$.

For the quantum reweight-annealing scheme, we adopt a similar procedure as introduced above. For $Z(s_{k-1})/Z(s_k) = \langle (s_{k-1}/s_k)^{n_{k,odd}} \rangle_{s_k}$, we can expect that when $s \rightarrow 0$, the number of the operators of the bonds with odd indices goes to zero in Eq. (3). Therefore we can

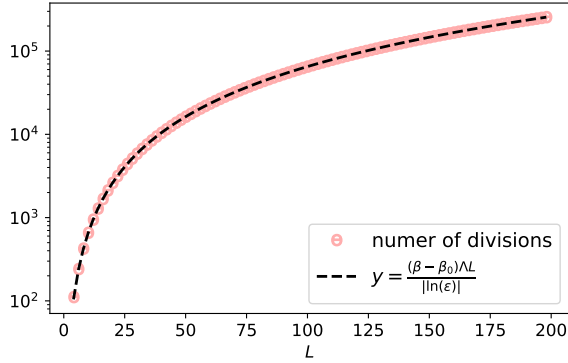


FIG. 1. The number of divisions in the T-Re-An method of first example in our paper, where we take $\beta = 30$ and $\Lambda = L$.

take $n_{k,\text{odd}} \approx \tilde{n}_{k,\text{odd}} = \Gamma_k \beta s_k L$ ($\Gamma_k \beta s_k L^2$) for 1D (2D) system, and we find this hypothetical linear relation on s is convenient and has sufficiently good performance. The number of divisions in this case similarly scales with $\mathcal{O}(\Gamma \beta L)$ for some uniform $\Gamma_k = \Gamma$ if in 1D system.

(III) Computing entanglement entropy

One important application of our method is to calculate the entanglement entropy in conjunction with the Bisognano-Wichmann theorem, which offers an excellently approximated functional form to the entanglement Hamiltonian in systems exhibiting translational symmetry. We briefly introduce the functional form of 1D/2D system with periodic boundary condition here.

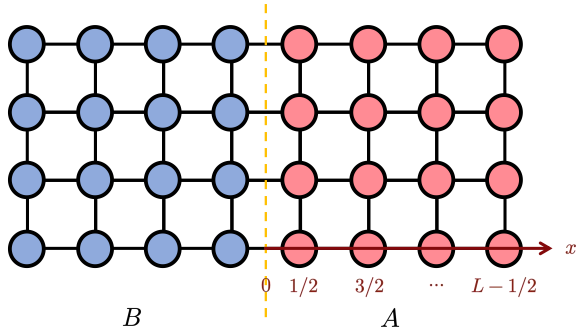


FIG. 2. Illustration of the LBW Hamiltonian with an example of a 2D square lattice with size $2L \times L$ under half bipartition. The d in Eq. (14) denotes the distance from the corresponding site/bond to the boundary (the orange dashed line). The spacing of lattice is taken to be 1.

As it shown in Fig. 2, for an 1D/2D system under

half bipartition (cornerless) with A and B part, if the Hamiltonian takes the form

$$H = \Gamma \sum_{x,y,\delta=\pm 1} [h_{(x,y),(x+\delta,y)} + h_{(x,y),(x,y+\delta)}] + \Theta \sum_{x,y} l_{(x,y)} \quad (12)$$

with nearest-neighbor coupling Γ and on-site coupling Θ , then the corresponding lattice Bisognano-Wichmann (LBW) Hamiltonian \tilde{H}_A is

$$\tilde{H}_A = \frac{2\pi}{v} \left[\sum_{x,y,\delta=\pm 1} [\Gamma_x h_{(x,y),(x+\delta,y)} + \Gamma_y h_{(x,y),(x,y+\delta)}] + \Theta_x \sum_{x,y} l_{(x,y)} \right] \quad (13)$$

where v denotes the sound velocity and Γ , Θ are modified to be Γ_x , Γ_y , and Θ_x . For period boundary condition, we have

$$\begin{aligned} \Gamma_{\delta=x,y} &= \frac{d(L-d)}{L} \\ \Theta_x &= \frac{d(L-d)}{L} \end{aligned} \quad (14)$$

which depend on the distance d to the boundary of the corresponding bond/site term (See Fig. 2).

With the LBW Hamiltonian \tilde{H}_A , we can define the LBW reduced density matrix $\tilde{\rho}_A$, which is

$$\tilde{\rho}_A \equiv \frac{e^{-\tilde{H}_A}}{\text{tr}\{e^{-\tilde{H}_A}\}} \approx \rho_A \quad (15)$$

where ρ_A is the real reduced density matrix. Therefore we can compute the Von Neumann entropy $S(\rho_A)$ by

$$S(\rho_A) \approx -\text{tr}\{\tilde{\rho}_A \ln \tilde{\rho}_A\} = \langle \tilde{H}_A \rangle + \ln \tilde{Z}_A \quad (16)$$

where $Z_A \equiv \text{tr}\{e^{-\tilde{H}_A}\}$. Attention that Eq. (16) is exactly the thermal entropy of \tilde{H}_A at $\beta = 1$. Since it requires the value of $\ln \tilde{Z}_A$, our method can thus be used to calculate the Von Neumann entropy of lattice systems with translational symmetry.

In addition to the LBW-HM model shown in the main body of the paper, we present another example of the 1D transverse field Ising model (TFIM), and calculate its Von Neumann entropy at the critical point with the reweight-annealing method. The exact result is $S(L) \propto (c/3) \ln L$, where $c = 0.5$ is the central charge, and our method gives $c \approx 0.501(4)$, as it shown in Fig. 3.

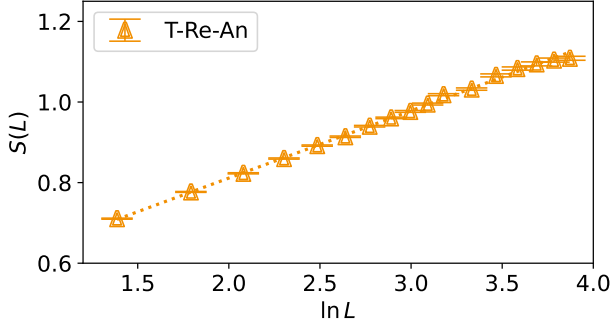


FIG. 3. For the 1D TFIM model at the critical point under PBC, the Von Neumann entropy obtained via calculating the thermal entropy of the corresponding BW-TFIM model at $\beta = 1$. The central charge extracted from our Re-An simulations is $c = 0.501(4)$, which is consistent with the theoretical result 0.5.